Chapter 5 : Conclusions

5.1 ADSORPTION

Based on the present study, the following conclusions were drawn:

1) Low cost materials like wood ash, appear to be suitable for the removal of nickel from electroplating and metal finishing wastewaters

2) An extensive experimental investigation was conducted to establish the adsorption behaviour of wood ash. The extent of metal removal depends significantly on the pH values used. By adjusting the temperature, pH of the solution and dose of the adsorbent, the nickel concentration in water can be reduced below the permissible limit (Appendix) even to zero concentration, at low level concentrations of nickel in water.

3) The kinetics of adsorption can be determined at low levels of nickel in polluted waters utilizing the wood ash. Maximum removal of nickel at 0.017 m.mol/L was observed in the pH range of 4.5-5.5. The data may be useful for future studies of the same.

4) The effects of pH can be attributed to the electrostatic interaction between the charged adsorbate species and the surface of the wood ash.

5) The sorption reaction can be described by the simple first order unimolecular reversible reaction. The reversible rate constants have been evaluated for wood ash.

6) The sorption equilibrium data can be approximated to both the Langmuir and Freundlich isotherms. The equilibrium data obtained at pH 5 and 30 C indicate

that the maximum adsorption capacity of the wood ash for nickel is 0.492 m.mol/g.

7) The presence of common interferences such as salts of anions and cations hindered the adsorption process, thereby lowering the adsorption capacity for the heavy metals. However, further studies are required with higher cation to heavy metals ratios in order to confirm the result reported here. The present work has been carried out using low cation to heavy metals ratios.

that the maximum adsorption capacity of the wood ash for nickel is 0.492 m.mol/g.

7) The presence of common interferences such as salts of anions and cations hindered the adsorption process, thereby lowering the adsorption capacity for the heavy metals. However, further studies are required with higher cation to heavy metals ratios in order to confirm the result reported here. The present work has been carried out using low cation to heavy metals ratios.

5.2 MEMBRANE SEPARATION

The present work aimed to determine the effect of trans-membrane pressure on the permeate flux for Ni(SO4)2. The concentration of Ni(II) which was used in this study reflects the concentration of Ni(II) in electroplating wastewaters in Malaysia.

The performance of the system in relation to process water reclamation was dependent on the trans-membrane pressure.In this work, a spirial wound cellulose acetate membrane module was used (model FT30, Filmtec Membrane) for concentrating the heavy metals and recovering high-purity process water. The delivery pressure of the pump was a limiting factor in controlling the trans-membrane pressure. Owing to this constraint the trans-membrane pressue was restricted in the range of 100.0 kPa to 600.0 kPa. At low trans-membrane pressure, the flow became too strong and the unit was opeated in a bypass mode. This caused a vortex in the feed tank and resulted in fluctuations in results.

For this equipment, the maximum attainable flow rate is 8.0×10^{-5} m^3/s. The maximum flow rate (7.75×10^{-5} m^3/s at 550.0 kPa) was maintained for $Ni(SO_4)_2$.

The various concentration of the salts, namely 10 mg/L, 30 mg/L and 50 mg/L did not have much baring on the trans-membrane pressure drop vs. permeate flow rate characteristics.

For example, corresponding to a permeate flow rate 7.75 x 10^{-5} m^3/s , the trans-membrane pressure drop was 490.0 kPa for the concentration of 10 mg/L and 550.0 kPa for both 30 mg/L and 50 mg/L. The reason for such aberrations are not clear. It is possible that due to fluctuations in trans-membrane pressure at the highest admissible flow rate, the time averaged recording was not accurate. On the other hand, at the lower end of the permeate flux (4.42 x 10^{-5} m^3/s) the trans-membrane pressure drop was 100 kPa. The permeate flow rate was same at this lower end but the amount of Ni(II) was different in the permeate for different concentrations.

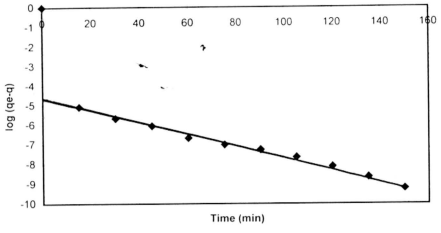

Fig. 4.3.a : First order reversible kinetic fit of Ni(II) adsorption data, on wood ash, at 0.17 mMol/L solution concentration.

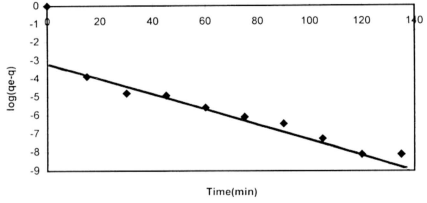

Fig. 4.3.b : First order reversible kinetic fit of Ni(II) adsorption data, on wood ash, at 0.345 mMol/L solution concentration.

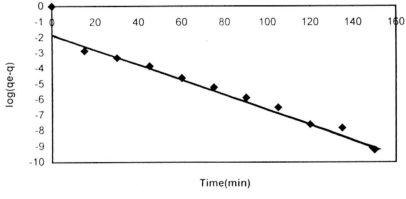

Fig. 4.3.c : First order reversible kinetic fit of Ni(II) adsorption data, on wood ash, at 0.603 mMol/L solution concentration.

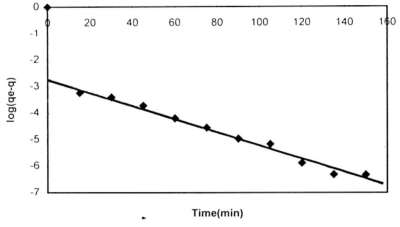

Fig. 4.3.d : First order reversible kinetic fit of Ni(II) adsorption data, on wood ash, at 0.86 mMol/L solution concentration.

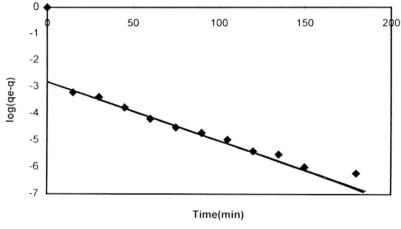

Fig. 4.3.e : First order reversible kinetic fit of Ni(II) adsorption data, on wood ash, at 1.21 mMol/L solution concentration.

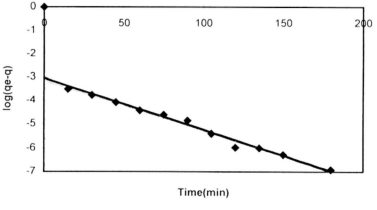

Fig. 4.3.f : First order reversible kinetic fit of Ni(II) adsorption data, on wood ash, at 1.55 mMol/L solution concentration.

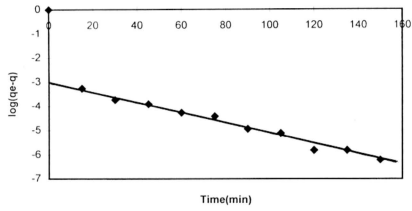

Fig. 4.3.g : First order reversible kinetic fit of Ni(II) adsorption data, on wood ash, at 1.72 mMol/L solution concentration.

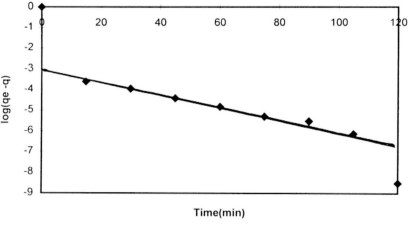

Fig.4.3.h : First order reversible kinetic fit of Ni(II) adsorption data, on wood ash, at 1.98 mMol/L solution concentration.(Condition: Tem 30 C & pH 5)

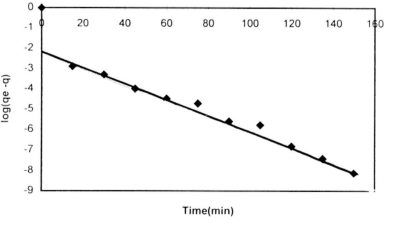

Fig. 4.3.i : First order reversible kinetic fit of Ni(II) adsorption data, on wood ash, at 2.07 mMol/L solution concentration.

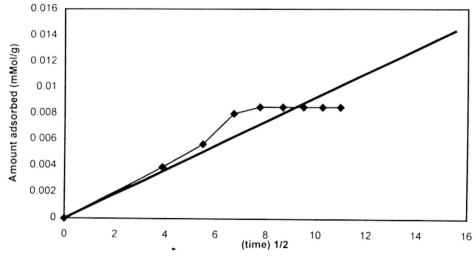

Fig.4.4.1a: Plot for rate constant of pore diffusion at 0.17 mMol/L s concentration. (Condition: Temp. 20°C & pH 5)

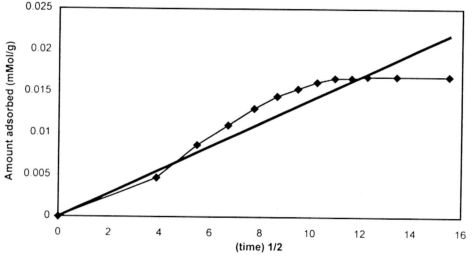

Fig.4.4.1b: Plot for rate constant of pore diffusion at 0.345 mMol/L concentration. (Condition: Temp. 20°C & pH 5)

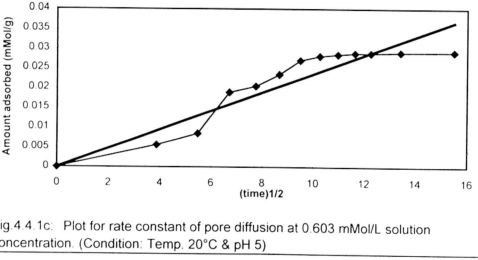

Fig.4.4.1c: Plot for rate constant of pore diffusion at 0.603 mMol/L solution concentration. (Condition: Temp. 20°C & pH 5)

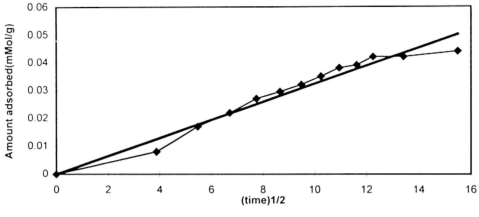

Fig.4.4.1d: Plot for rate constant of pore diffusion at 0.86 mMol/L solution concentration. (Condition: Temp. 20°C & pH 5)

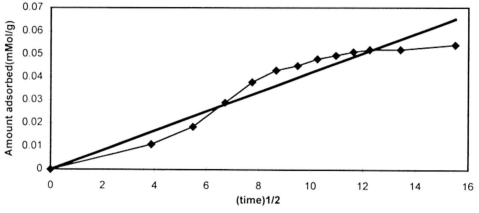

Fig.4.4.1e: Plot for rate constant of pore diffusion at 1.21 mMol/L solution concentration. (Condition: Temp. 20°C & pH 5)

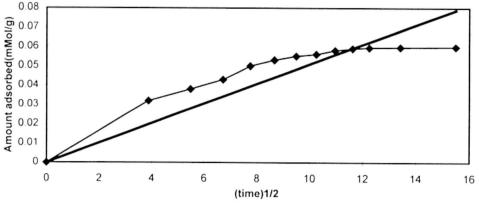

Fig.4.4.1f: Plot for rate constant of pore diffusion at 1.55 mMol/L solution Concentration. (Condition: Temp. 20°C & pH 5)

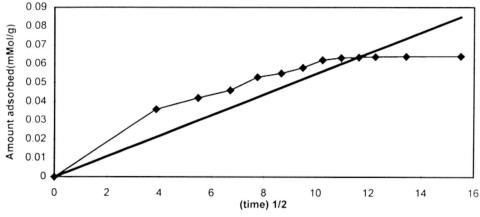

Fig.4.4.1g: Plot for rate constant of pore diffusion at 1.72 mMol/L solution concentration. (Condition: Temp. 20°C & pH 5)

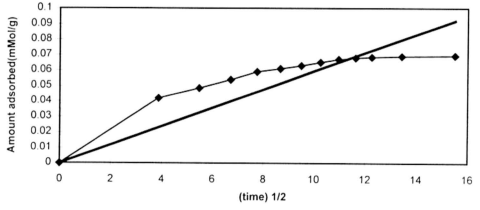

Fig.4.4.1h: Plot for rate constant of pore diffusion at 1.98 mMol/L solution concentration. (Condition: Temp. 20°C & pH 5)

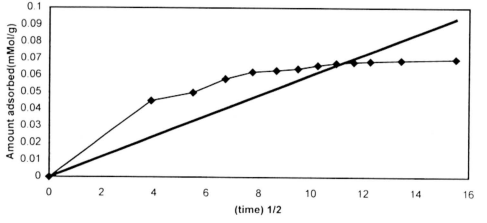

Fig.4.4.1i: Plot for rate constant of pore diffusion at 2.07 mMol/L solution concentration. (Condition: Temp. 20°C & pH 5)

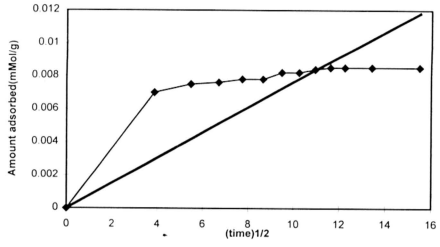

Figure 4.4.2a. Plot for rate constant of pore diffusion at 0.17mMol/L solution concentration (Cond. Temp. 30°C &pH 5)

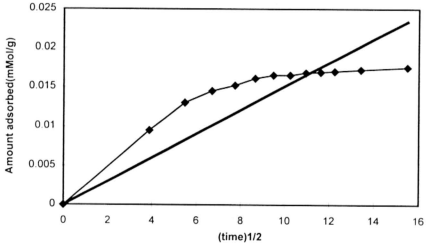

Figure 4.4.2b: Plot for rate constant of pore diffusion at 0.345 mMol/L solution concentration (Cond. Temp.30°C &pH 5)

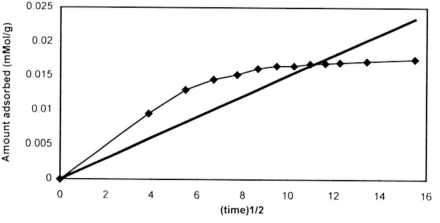

Figure 4.4.2c: Plot for rate constant of pore diffusion at 0.603 mMol/L solution concentration(Cond. Temp. 30°C &pH 5)

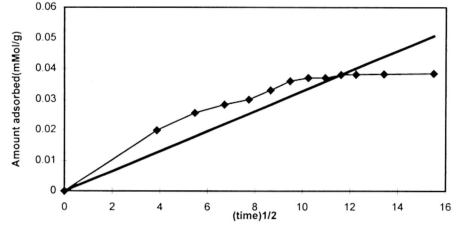

Figure 4.4.2d. Plot for rate constant of pore diffusion at 0.86 mMol/L solution concentration (Cond. Temp.30° C &pH 5)

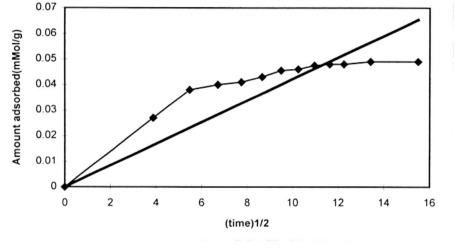

Figure 4.4.2e. Plot for rate constant of pore diffusion at 1.21mMol/L solution concentration (Cond.Temp.30° &pH 5)

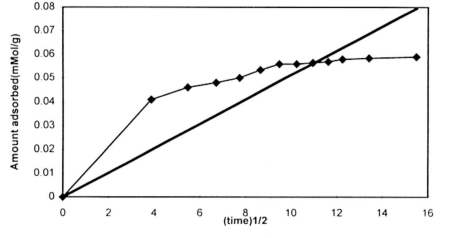

Figure 4.4.2f. Plot for rate constant of pore diffusion at 1.55 mMol/L solution concentration (Cond. Temp.30° C &pH 5)

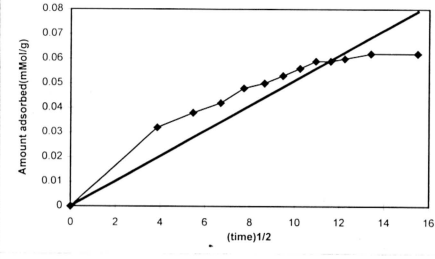

Figure 4.4.2g. Plot for rate constant of pore diffusion at 1.72 mMol/L solution concentration (Cond. Temp.30° C &pH 5)

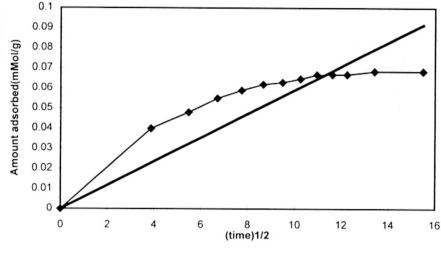

Figure 4.4.2h. Plot for rate constant of pore diffusion at 1.98 mMol/L solution concentration (Cond. Temp.30°C &pH 5)

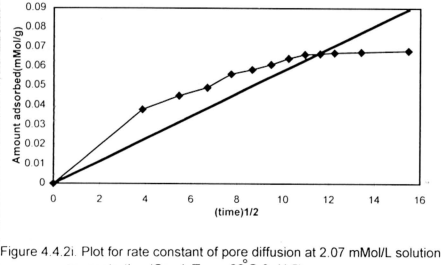

Figure 4.4.2i. Plot for rate constant of pore diffusion at 2.07 mMol/L solution concentration (Cond. Temp.30° C &pH 5)

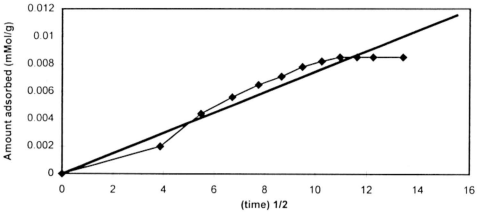

Fig.4.4.3a: Plot for rate constant of pore diffusion at 0.17 mMol/L solution concentration. (Condition: Temp. 40°C & pH 5)

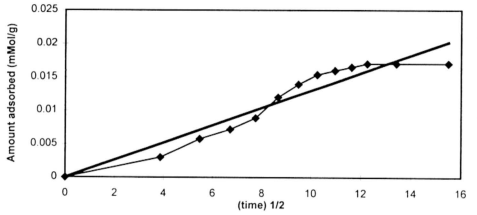

Fig.4.4.3b: Plot for rate constant of pore diffusion at 0.345 mMol/L solution concentration. (Condition: Temp. 40°C & pH 5)

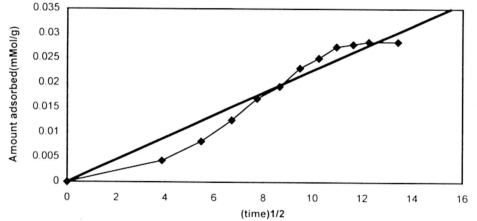

Fig.4.4.3c: Plot for rate constant of pore diffusion at 0.603 mMol/L solution concentration. (Condition: Temp. 40°C & pH 5)

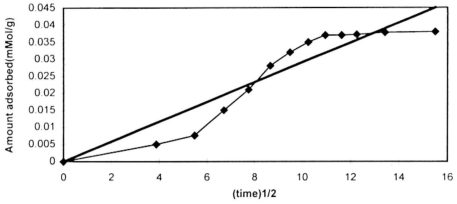

Fig.4.4.3d: Plot for rate constant of pore diffusion at 0.86 mMol/L solution concentration. (Condition: Temp. 40°C & pH 5)

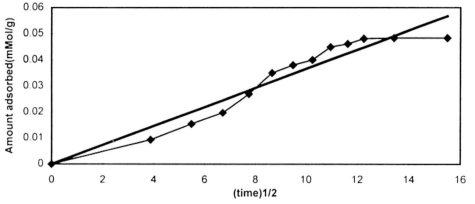

Fig.4.4.3e: Plot for rate constant of pore diffusion at 1.21 mMol/L solution concentration. (Condition: Temp. 40°C & pH 5)

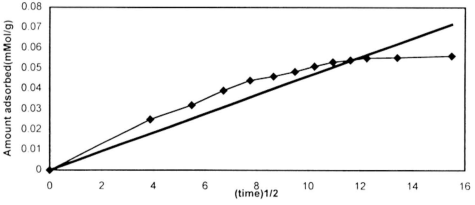

Fig.4.4.3f: Plot for rate constant of pore diffusion at 1.55 mMol/L solution concentration. (Condition: Temp. 40°C & pH 5)

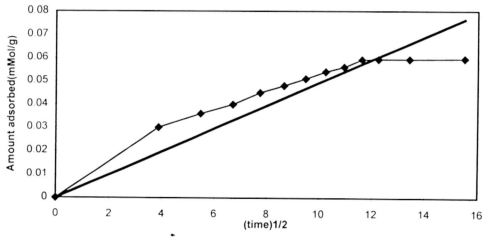

Fig. 4.4.3g : Plot for rate constant of pore diffusion at 1.72 mMol/L solution Concentration Cond. Temp. 40°C & pH 5

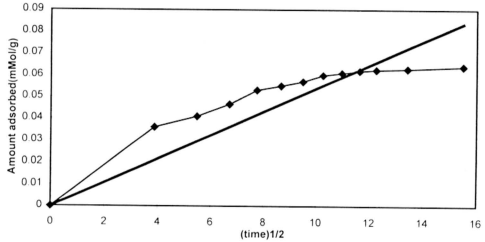

Fig. 4.4.3h : Plot for rate constant of pore diffusion at 1.98 mMol/L solution Concentration Cond. Temp. 40°C & pH 5

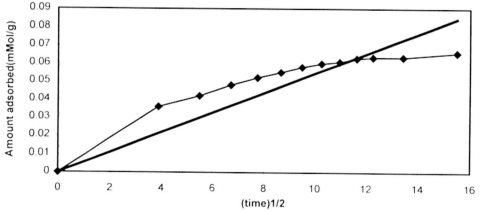

Fig.4.4.3i : Plot for rate constant of pore diffusion at 2.07 mMol/L solution Concentration Cond. Temp. 40°C & pH 5

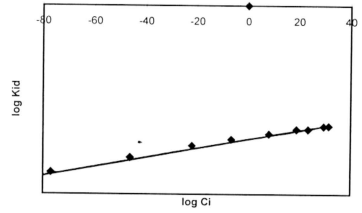

Figure 4.5: Log-log plot of rate parameters(Kid) against initial Ni(ii) concentration.

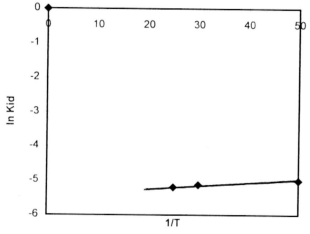

Figure 4.6: Arrhenius plot for the determination of activation energy.

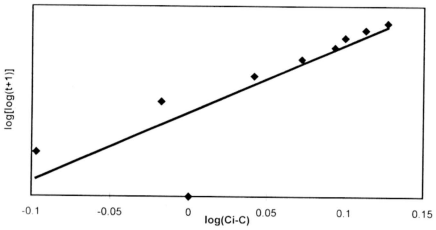

Fig. 4.7.a: Plot for the determination of empirical constants B and A at 2.07 mMol/L solution concentration.

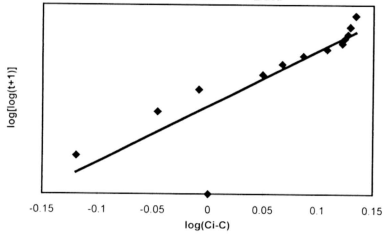

Fig. 4.7.b: Plot for the determination of empirical constants B and A at 1.98 mMol/L solution concentration.

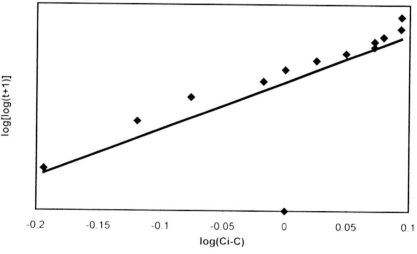

Fig. 4.7.c: Plot for the determination of empirical constants B and A at 1.72 mMol/L solution concentration.

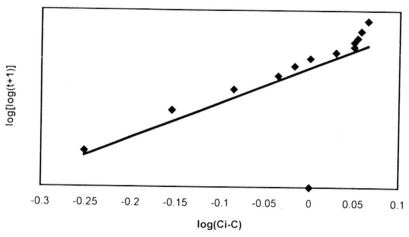

Fig. 4.7.d: Plot for the determination of empirical constants B and A at 1.55 mMol/L solution concentration.

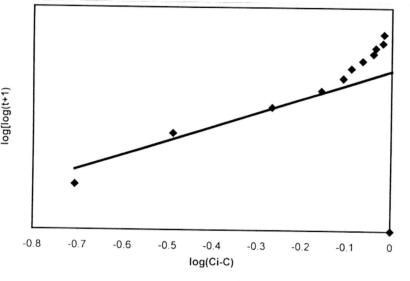

Fig. 4.7.e: Plot for the determination of empirical constants B and A at 1.21 mMol/L solution concentration.

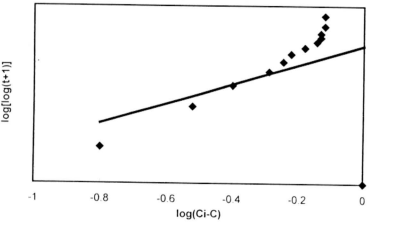

Fig. 4.7.f: Plot for the determination of empirical constants B and A at 0.86 mMol/L solution concentration.

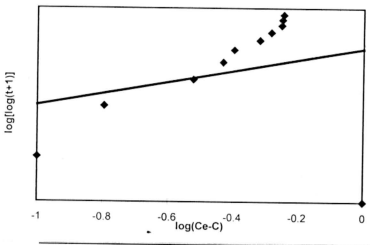

Fig. 4.7.g: Plot for the determination of empirical constants B and A at .603 mMol/L solution concentration.

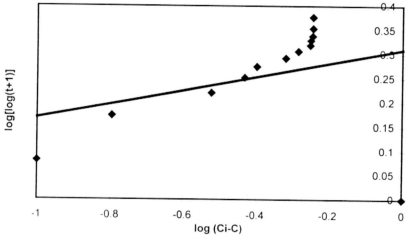

Fig. 4.7.h: Plot for the determination of empirical constants B and A at .345 mMol/L solution concentration.

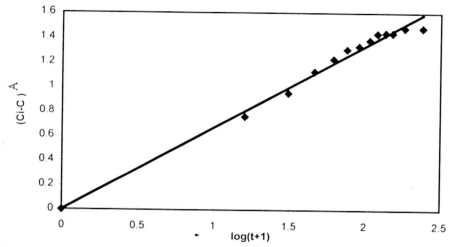

Fig. 4.8.a: Plot for the kinetics of Ni(II) removal at 2.07 mMol/L solution concentration.

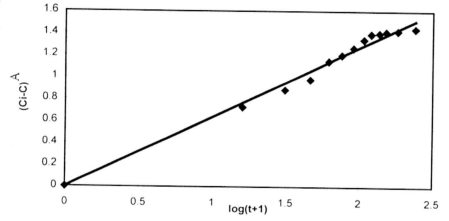

Fig. 4.8.b: Plot for the kinetics of Ni(II) removal at 1.98 mMol/L solution concentration.

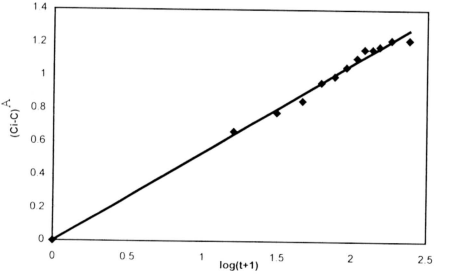

Fig. 4.8.c: Plot for the kinetics of Ni(II) removal at 1.72 mMol/L solution concentration.

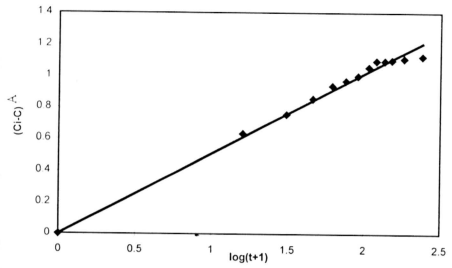

Fig. 4.8.d: Plot for the kinetics of Ni(II) removal at 1.55 mMol/L solution concentration.

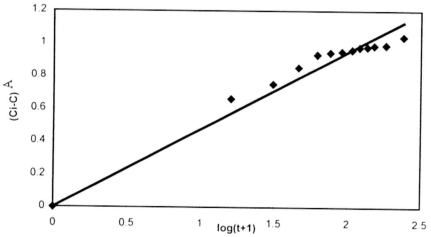

Fig. 4.8.e: Plot for the kinetics of Ni(II) removal at 1.21 mMol/L solution concentration.

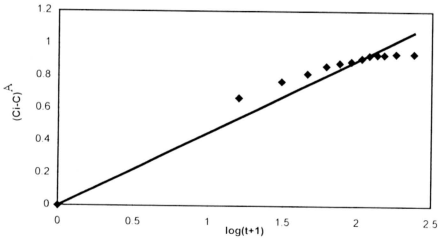

Fig. 4.8.f: Plot for the kinetics of Ni(II) removal at 0.86 mMol/L solution concentration.

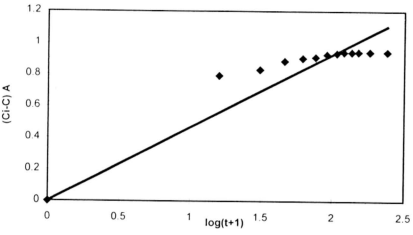

Fig. 4.8.g: Plot for the kinetics of Ni(II) removal at 0.603 mMol/L solution concentration.

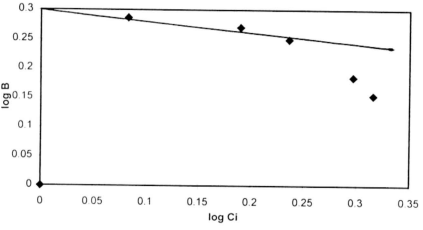

Fig. 4.9 : Variation of logB with log Ci

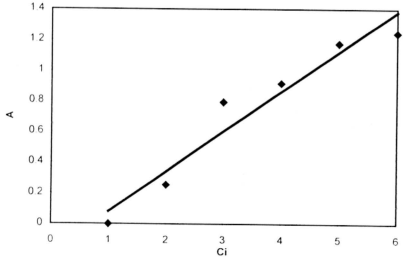

Fig. 4.10 : Variation of A with initial concentration

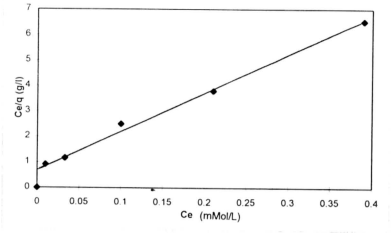

Fig. 4.11 : Langmuir plot at 30° C temperature

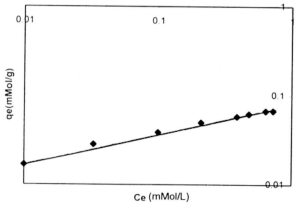

Fig. 4.12 Freundlich Isotherm plot at 30° C temperature.

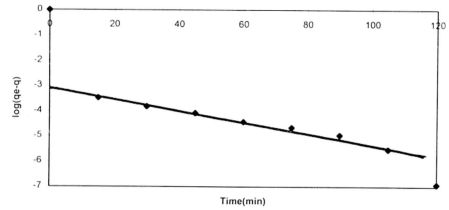

Fig. 4.13.d : First order reversible kinetic fit of Ni(II) adsorption on wood ash at 0.86 mMol/L solution concentration.(Cond. Temp. 40°C & pH 5)

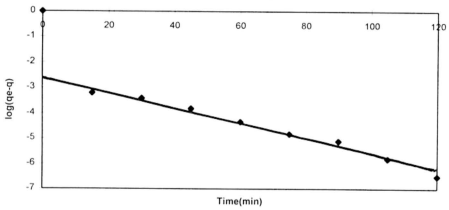

Fig. 4.13.e : First order reversible kinetic fit of Ni(II) adsorption on wood ash at 1.21 mMol/L solution concentration.(Cond. Temp. 20°C & pH 5)

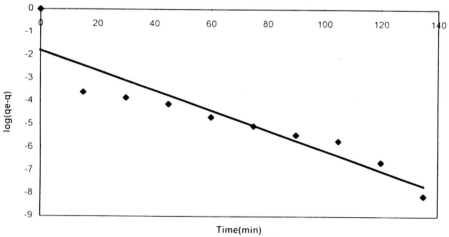

Fig. 4.13.f : First order reversible kinetic fit of Ni(II) adsorption on wood ash at 1.55 mMol/L solution concentration.(Cond. Temp. 20°C & pH 5)

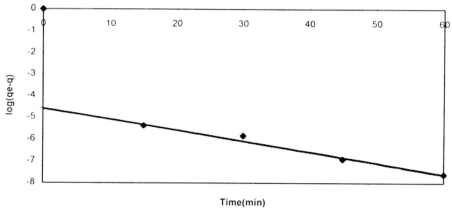

Fig. 4.13.a : First order reversible kinetic fit of Ni(II) adsorption data, on wood-ash at 0.17mMol/L solution concentration.(Cond. Temp. 20° C & pH 5)

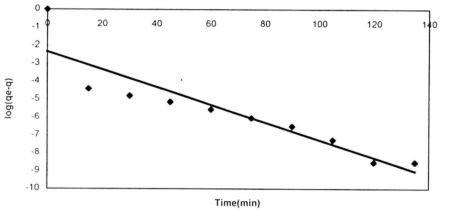

Fig. 4.13.b : First order reversible kinetic fit of Ni(II) adsorption data, on wood-ash at 0.345mMol/L solution concentration.(Cond. Temp. 20° C & pH 5)

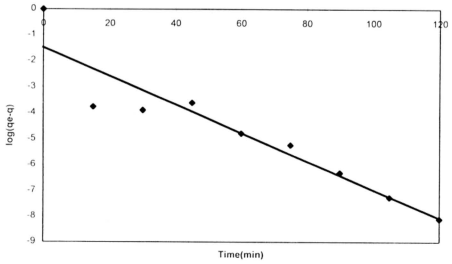

Fig. 4.13.c : First order reversible kinetic fit of Ni(II) adsorption data, on wood-ash at 0.603mMol/L solution concentration.(Cond. Temp. 20° C & pH 5)

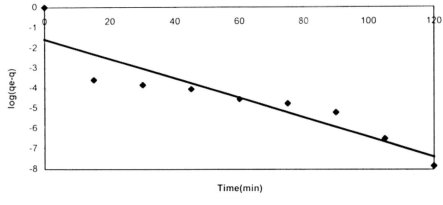

Fig. 4.13.g : First order reversible kinetic fit of Ni(II) adsorption on wood ash at 1.72 mMol/L solution concentration.(Cond. Temp. 40°C & pH 5)

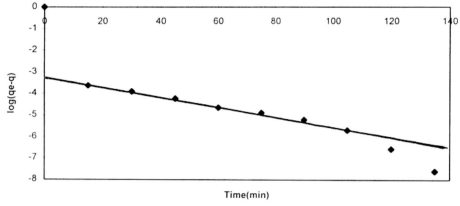

Fig. 4.13.h : First order reversible kinetic fit of Ni(II) adsorption on wood ash at 1.98 mMol/L solution concentration.(Cond. Temp. 20°C & pH 5)

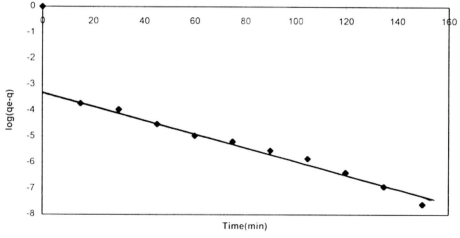

Fig. 4.13.i : First order reversible kinetic fit of Ni(II) adsorption on wood ash at 2.07 mMol/L solution concentration (Cond. Temp.20°C & pH 5)

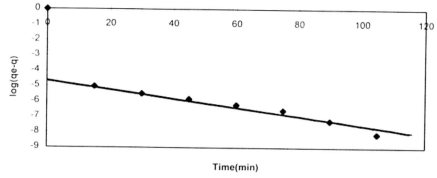

Fig.4.14.a : First order reversible kinetic fit of Ni(II) adsorption on wood-ash at 0.17 mMol/L solution concentration.(Cond. Temp.40° C &pH 5)

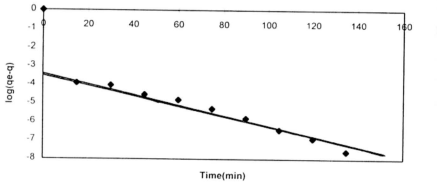

Fig.4.14.b : First order reversible kinetic fit of Ni(II) adsorption on wood-ash at 0.345 mMol/L solution concentration.(Cond. Temp.40° C &pH 5)

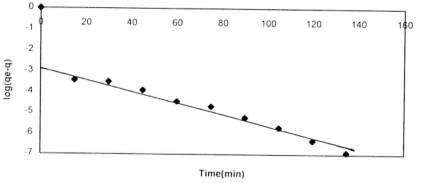

Fig.4.14.c : First order reversible kinetic fit of Ni(II) adsorption on wood-ash at 0.603 mMol/L solution concentration.(Cond. Temp.40° C &pH 5)

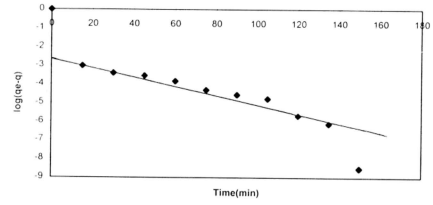

Fig.4.14.d : First order reversible kinetic fit of Ni(II) adsorption on wood-ash at 1.21 mMol/L solution concentration.(Cond. Temp.40°C &pH 5)

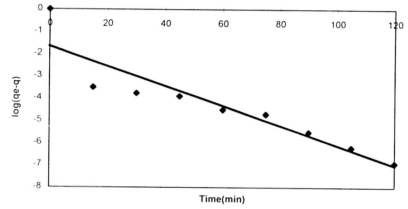

Fig.4.14.e : First order reversible kinetic fit of Ni(II) adsorption on wood-ash at 1.55 mMol/L solution concentration.(Cond. Temp.40°C &pH 5)

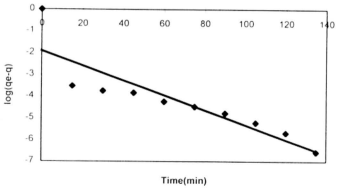

Fig.4.14.f : First order reversible kinetic fit of Ni(II) adsorption on wood-ash at 1.72 mMol/L solution concentration.(Cond. Temp.40°C &pH 5)

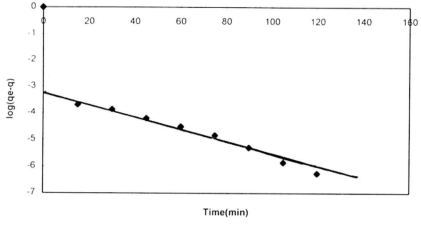

Fig.4.14.g : First order reversible kinetic fit of Ni(ii) adsorption on wood-ash at 1.98 mMol/L solution concentration.(Cond. Temp.40 °C &pH 5)

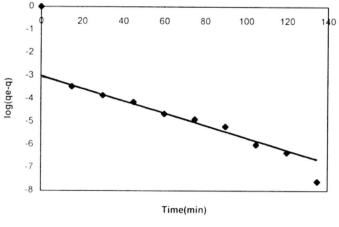

Fig.4.14.h : First order reversible kinetic fit of Ni(ii) adsorption on wood-ash at 2.07 mMol/L solution concentration.(Cond. Temp.40 °C &pH 5)

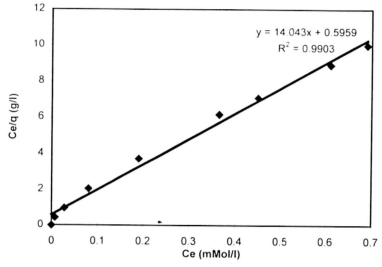

Fig. 4.15: Langmuir plot at 20 C

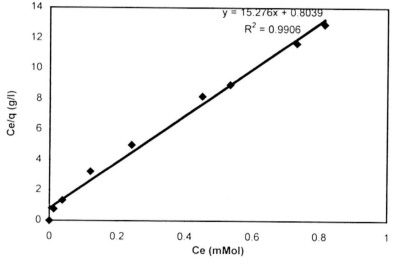

Fig. 4.16 Langmuir plot at 40 C

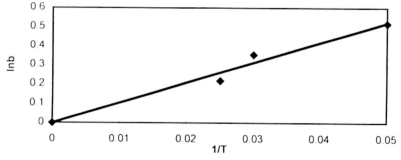

Fig. 4.17 Plot for the calculation of apparant heat of adsorption

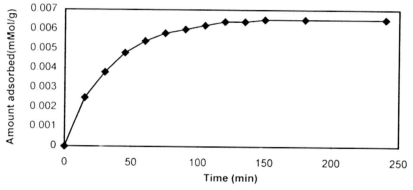

Fig.4.19 : Effect of chloride on Ni(II) adsorption by wood-ash.
(Cond. Temp. 30°C & 0.017mMol/L solution concentration.)

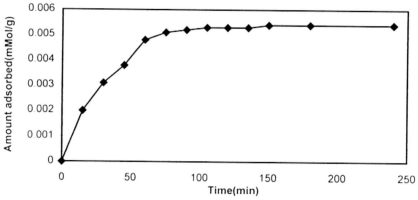

Fig. 4.20 : Effect of sulfate on Ni(II) adsorption by wood-ash.
(Cond. Temp. 30°C & 0.017mMol/L solution concentration.)

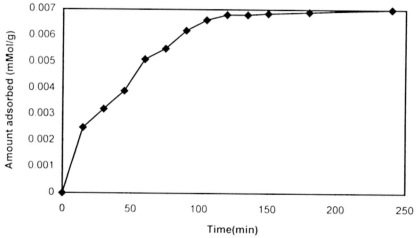

Fig. 21 : Effect of EDTA on Ni(II) adsorption by wood-ash.
(Cond. Temp. 30°C & 0.017mMol/L solution concentration.)

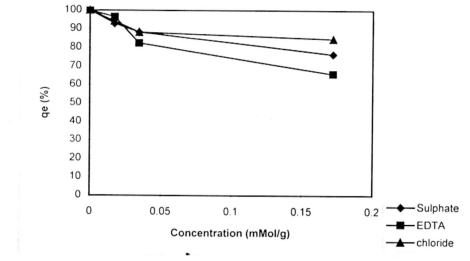

Fig. 4.22 : Effect of anions on Ni(ii) adsorption by wood-ash.
(Cond. Temp. 30°C & 0.017mMol/L solution concentration.)

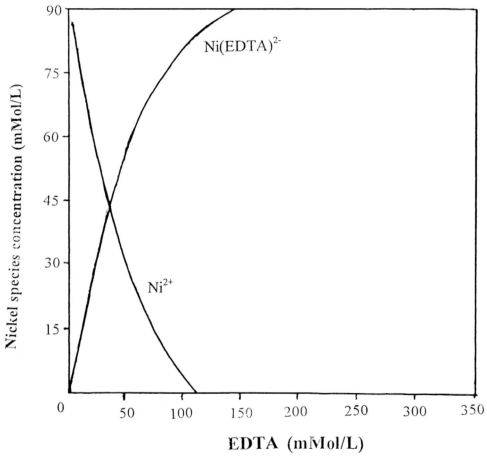

Fig. 4.23 Nickel speciation at varying concentrations of EDTA. Initial nickel concentration = 0.17 mMol/L, pH = 5.0

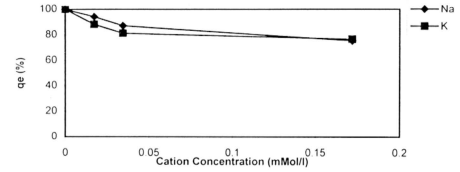

Fig. 4.24 : Effects of cation on adsorption by wood-ash.
(Cond. Temp. 30°C & 0.017mMol/L solution concentration.)

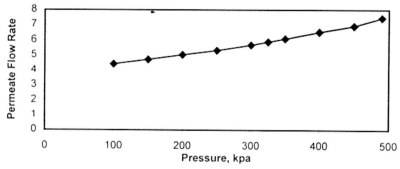

Fig.4.25(a)

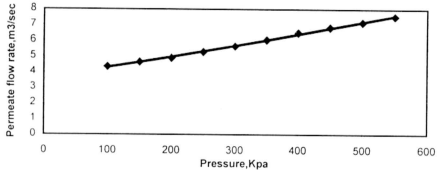

Fig. 4.25(b)

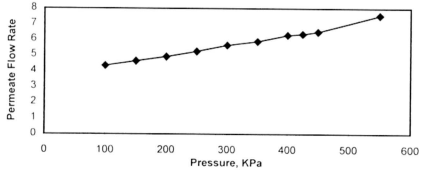

Fig.4.25.(c)

Fig. 4.25 : Relationship between trans-membrane pressure drop(TMP) and permeate flow rate.

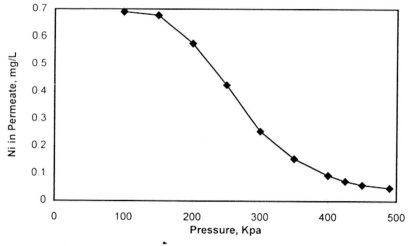

4.26 (a)

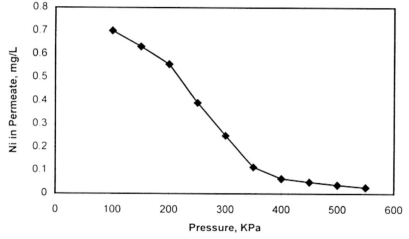

4.26 (b)

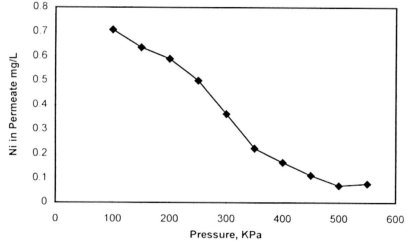

Fig. 4.26(c)

Fig.4.26 : Relationship between trans-membrane pressure drop (TMP) and Ni in Permeate.

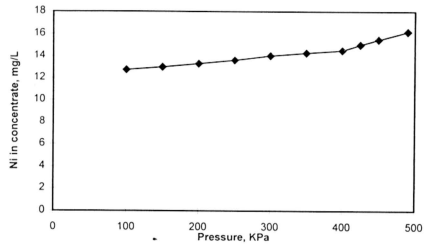

Fig. 4.27 (a)

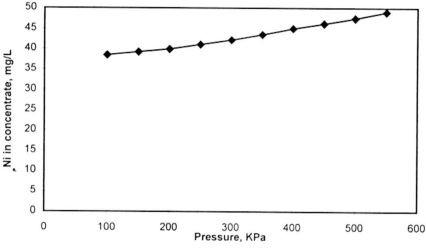

Fig. 4.27 (b)

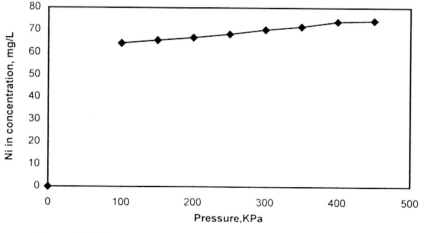

Fig. 4.27 (c)

Fig. 4.27: Trans membrane Pressure vs.Ni(ii) in Concentrate

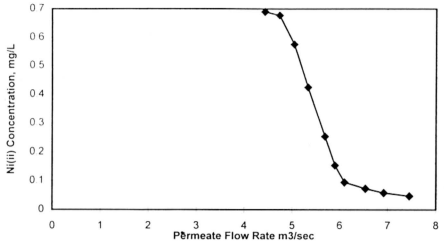

4.28 (a)

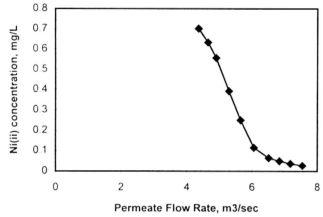

Fig. 4.28 (b)

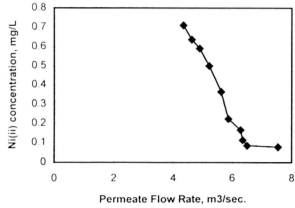

Fig. 4.28 (c)

Fig. 4.28 : Relationship between flowrate and Ni(ii) in Permeate.

Material Balance

Basis:
Feed : 700 L/h
Feed Concentration : 10 mg/L

Pressure KPa	Total Feed L/h	Permeate L/h	Concentrate L/h	Ni(ii) in Permeate mg/L	Ni(ii) in Concentrate mg/L
100	700	159.34	540.66	0.69	12.7438
150		170.28	529.72	0.678	12.9966
200		181.44	518.56	0.576	13.2974
250		191.88	508.12	0.425	13.6158
300		204.84	495.16	0.255	14.0314
350		212.4	487.6	0.155	14.2884
400		219.6	480.4	0.095	14.5278
425		235.44	464.56	0.0735	15.0307
450		249.12	450.88	0.059	15.4926
490		268.2	431.8	0.048	16.1814

Basis:
Feed : 700 L/h
Feed Concentration : 30 mg/L

Pressure KPa	Total Feed L/h	Permeate L/h	Concentrate L/h	Ni(ii) in Permeate mg/L	Ni(ii) in Concentrate mg/L
100	700	156.96	543.04	0.7013	38.4685
150		167.40	532.6	0.6325	39.2304
200		176.4	523.6	0.5569	39.9193
250		190.44	509.56	0.3924	41.0654
300		203.4	496.6	0.2501	42.1851
350		218.04	487.96	0.1148	43.5201
400		234.44	473.56	0.0648	45.0743
450		246.28	466.72	0.05	46.2569
500		258.2	458.8	0.0379	47.5106
550		271.44	428.56	0.0276	48.9838

Basis:
Feed : 700 L/h
Feed Concentration : 50 mg/L

Pressure KPa	Total Feed L/h	Permeate L/h	Concentrate L/h	Ni(ii) in Permeate mg/L	Ni(ii) in Concentrate mg/L
100	700	156.24	543.76	0.7097	64.1627
150		166.68	533.32	0.6368	65.4276
200		176.4	523.6	0.5908	66.6459
250		187.92	512.08	0.5	68.1652
300		202.32	497.68	0.3638	70.1784
350		211.32	488.68	0.2231	71.5250
400		226.08	473.92	0.1662	73.7728
450		228.6	471.4	0.113	74.1921
500		234	466	0.07	75.0665
550		271.44	428.56	0.078	81.6194